

# Environmentally Friendly Synthesis of Magnetic $\text{CuFe}_2\text{O}_4$ Powder as Photo-Fenton Catalysts by Sol-Gel Method Using Tamarind Fruit Extract

Bao Luu Gia Nguyen<sup>a</sup>, Trinh Thi Tran Thi<sup>b, c</sup>, Quoc Thiet Nguyen<sup>d</sup>, and Tien Khoa Le<sup>b, c, \*</sup>

<sup>a</sup> International School of Ho Chi Minh City, Ho Chi Minh City, Vietnam

<sup>b</sup> Faculty of Chemistry, University of Science, Ho Chi Minh City, Vietnam

<sup>c</sup> Faculty of Chemistry, University of Science, Vietnam National University, Ho Chi Minh City, Vietnam

<sup>d</sup> Institute of Applied Materials Science, Vietnam Academy of Science and Technology, Ho Chi Minh City, Vietnam

\*e-mail: [ltkhoa@hcmus.edu.vn](mailto:ltkhoa@hcmus.edu.vn)

Received September 20, 2022; revised November 5, 2022; accepted November 26, 2022

**Abstract**—The present paper reports the synthesis of magnetic photo-Fenton catalysts based on  $\text{CuFe}_2\text{O}_4$  via an environmentally friendly sol-gel method at different annealing temperatures (700, 800, and 900°C) using tamarind fruit extract as a chelating agent. The catalysts were characterized by X-ray diffraction, scanning electron microscopy, nitrogen adsorption, Fourier-transform infrared spectroscopy, and vibrating sample magnetometry. Their photo-Fenton catalytic performance was tested with oxalic acid for the degradation of Methylene Blue under UVA light and under visible light. According to the results, the annealing temperature was found to be the important factor, significantly affecting the oxalic acid-induced-photo-Fenton activity. When the annealing temperature increased from 700 to 800°C, the catalytic performance was strongly improved, which can be explained by the enhanced  $\text{Fe}^{3+}$  content on the catalyst surface. At higher annealing temperature, due to the growth and agglomeration of particles, the specific surface area was decreased, consequently reducing the catalytic activity. The sample prepared at 800°C also displayed good ferromagnetic properties, making it the most promising recyclable material for wastewater treatment in this study.

**Keywords:** tamarind fruit extract, sol-gel method,  $\text{CuFe}_2\text{O}_4$ , magnetic powder, photo-Fenton catalysis

**DOI:** 10.3103/S1063455X23030074

## INTRODUCTION

For the long time, copper ferrite ( $\text{CuFe}_2\text{O}_4$ ) with cubic and tetragonal spinel structures has been widely studied owing to its potential applications, such as hydrogen gas sensor [1], magnetic storage devices [2], electromagnetic and spintronic devices [3]. In particular, this material was also considered as an efficient magnetic catalyst for the treatment of organic pollutants since it exhibits both high Fenton or photo-Fenton catalytic activities as well as good ferromagnetic properties which allows the facile separation from the solution after reactions [4, 5]. For instance, in our previous study, magnetic  $\text{CuFe}_2\text{O}_4$  powders were successfully applied as a promising Fenton catalyst for the removal of Methylene Blue in five consecutive experiments [6]. Gao et al. also detailed the excellent effectiveness of three-dimensional  $\text{CuFe}_2\text{O}_4$  in eliminating sulfonamide antibiotics from near-neutral water as a photo-Fenton catalyst [7]. Likewise,  $\text{CuFe}_2\text{O}_4$  can be combined with graphene oxide to be more effective for the peroxymonosulfate-induced catalytic degradation of metronidazole [8]. From these works, various techniques including co-precipitation method [8], hydrothermal route [9], sol-gel method [4], and polymeric precursor method [10], have been employed to prepare copper ferrite. However, most of these synthesis methods require complicated procedures, expensive instrumental set-up and potential hazardous chemicals.

Hence, there is always a great demand for the synthesis of  $\text{CuFe}_2\text{O}_4$  by other environmentally friendly ways with simple equipment and benign reagents. Recently, some researchers have attempted to prepare  $\text{CuFe}_2\text{O}_4$  through a green chemistry approach using naturally available and less costly products such as Neem leaf extract [11] or *Morus alba* L. leaf extract [12]. These plant extracts usually contain a wide range of constituents such as carbohydrates, terpenoids, flavonoids, carboxylic acids... which function as cap-

ping or/and chelating agents for the preparation. One of the natural sources that could be used for the green synthesis of spinel materials is the tamarind fruit extract. Tamarind, known scientifically as *Tamarindus indica* L, is a leguminous tree bearing edible fruit which can be found in many tropical regions (South East Asia, India, Eastern Africa, etc.). Its fruit extract mainly contains tartaric acid (8–18%), reducing sugars, B-vitamins and proteins [13]. It was reported that the ingredients in the tamarind fruit extract are able to form polynuclear complex precursors with numerous metal ions, facilitating the synthesis of mixed-metal oxides like spinel-structured materials [14]. However, according to our best knowledge, there is still no report on the preparation of photo-Fenton catalyst based on  $\text{CuFe}_2\text{O}_4$  using the tamarind fruit extract.

Therefore, in this work, we proposed to synthesize magnetic  $\text{CuFe}_2\text{O}_4$  powders by the tamarind fruit extract-assisted sol-gel method at different annealing temperatures and then investigated the effects of annealing temperatures on their photo-Fenton catalytic activity induced by oxalic acid under UVA and visible light. The influences of annealing temperatures on the crystal structure, phase composition, morphology, surface functional groups and magnetic properties of these materials were also discussed in detail.

## EXPERIMENTAL

### *Sample Preparation*

In our work, all chemicals and reagents were commercially available and employed as received without further purification. The synthesis of  $\text{CuFe}_2\text{O}_4$  samples by tamarind fruit extract-assisted sol-gel method at different annealing temperatures was carried out through the 2-stages procedure described by Mindru et al. [14] with some modifications. In the first stage, the tamarind fruit extract was prepared as follows. 18.00 g tamarind pulp (purchased from DUC VINH company, Vietnam) whose skin and seed were previously removed, were mixed with 300 mL distilled water. The mixture was heated to reflux for 1 h to obtain a red-brown solution. Then the solution was allowed to cool at room temperature and filtered to eliminate all types of solid waste.

For the second stage, 30 mL solution containing  $\text{Fe}_2(\text{SO}_4)_3$  (0.5 mol/L) and  $\text{CuSO}_4$  (0.5 mol/L) were added to the 300 mL tamarind fruit extract. The solution was continuously stirred at room temperature for 2 h and at 80°C for 3 h in a Memmert water bath to obtain a viscous solution. This viscous solution was then placed into a Memmert oven at 150°C during 7 h to effectuate the polycondensation and gelation that forms a brown gel. Next, the gel was ground into fine powder which was subsequently annealed in air at various temperatures (700, 800 and 900°C) for 2 h using a Nabertherm muffle furnace. Finally, the obtained solid powder was rinsed with distilled water, separated from the solution by using a magnet and dried again at 150°C for 1 h. In the following manuscript, the samples annealed at 700, 800 and 900°C are labelled as CuFeO-700, CuFeO-800 and CuFeO-900, respectively.

### *Characterization*

The crystallinity of magnetic catalysts prepared at different annealing temperatures was characterized by powder X-ray diffraction (XRD) method on an EMPYREAN (PANalytical) diffractometer using  $\text{Cu K}\alpha$  radiation ( $\lambda = 0.15406$  nm) at a scan rate of  $0.03^\circ \text{ s}^{-1}$ . From these XRD patterns, the mass fraction of each crystalline phase was calculated by the Rietveld refinement method using the Fullprof 2009 structure refinement software. A HITACHI S-4800 field scanning electron microscope (FE-SEM) with an acceleration voltage of 10 kV was used to observe the morphology and the particle size of CuFeO samples. Their specific surface area was estimated using the Brunauer–Emmett–Teller (BET) analysis in the nitrogen adsorption/desorption isotherms which were recorded on a NOVA 1000e analyzer (Quantachrome Instruments). The surface chemical bonds were characterized by Fourier-transform infrared spectra (FTIR) taken on a VERTEX 70 spectrometer (Bruker) with KBr pellets at room temperature in the  $4000\text{--}400$   $\text{cm}^{-1}$  wavenumber range. The magnetic parameters such as saturation magnetization ( $M_s$ ), coercivity ( $H_c$ ) and remanent magnetization ( $M_r$ ) of CuFeO samples were determined via their hysteresis loop obtained on a DMS 880 vibrating sample magnetometer (ADE Technologies) with the magnetic field varying from  $-16000$  to  $+16000$  Oe at room temperature.

### *Catalytic Tests*

The photo-Fenton catalytic performance of our magnetic CuFeO samples was evaluated by the oxalic acid-induced-degradation of Methylene Blue (MB) in aqueous solution. All catalytic tests were con-

**Table 1.** Phase composition of CuFeO-700, CuFeO-800, and CuFeO-900 samples

Phase	Fraction, %		
	CuFeO-700	CuFeO-800	CuFeO-900
CuFe <sub>2</sub> O <sub>4</sub> (I41/amd)	28.33	85.78	90.37
Hematite (R-3c)	46.83		
CuO (C2/c)	24.84	14.22	9.63

ducted at room temperature under ambient conditions. Generally, 0.5 g of catalysts were mixed with 250 mL stock solution containing both MB ( $2 \times 10^{-5}$  mol/L) and H<sub>2</sub>C<sub>2</sub>O<sub>4</sub> ( $10^{-3}$  mol/L) in a glass jacketed reaction beaker cooled by continuous water flow. This solution was regularly stirred for 60 min by a mechanic agitator in the dark in order to obtain the MB adsorption equilibrium. Then an ultraviolet A (UVA) light lamp (9W Radium 78) or a visible light lamp (9W Osram Dulux S) was used to irradiate the solution for the photo-Fenton catalytic processes. The distance between the lamp and the solution surface is about 10 cm. At given time intervals, 5 mL aliquots of MB solution were sampled and the catalytic powder was magnetically separated from the solution by a magnet.

Finally, the remnant MB concentration in these aliquots was determined using a Helios Omega UV-Vis spectrophotometer (Thermo Fisher Scientific) at 664 nm. Moreover, the concentrations of Cu<sup>2+</sup> and Fe<sup>3+</sup> ions derived from CuFeO-800 sample in the solution were measured by an AA-6300 double beam atomic absorption spectrometer (Shimadzu).

## RESULTS AND DISCUSSION

### *Phase Structures, Morphology and Surface Functional Groups*

Figure 1 compares the XRD patterns of our CuFeO samples prepared at different annealing temperatures 700, 800 and 900°C. Their phase composition is summarized in Table 1. It was observed that the annealing temperatures significantly affect not only the number of crystalline phases, but also their mass fraction in our samples. For CuFeO-700 sample, three crystalline phases are detected. Firstly, a series of diffraction peaks located at 18.3°, 30.0°, 34.7°, 36.0°, 43.9°, and 62.2° are well indexed to the tetragonal spinel phase of CuFe<sub>2</sub>O<sub>4</sub> (space group I41/amd, JCPDS no. 34-0425). Secondly, the diffraction peaks at 24.1°, 33.1°, 35.4°, 49.5°, and 53.9° can be assigned to the hematite phase of Fe<sub>2</sub>O<sub>3</sub> (space group R-3c, JCPDS no. 86-0550). The third phase is the tenorite phase of CuO (space group C 2/c, JCPDS no. 05-0661), identified by the diffraction peaks at 38.5° and 48.6°. It should be noted that the mass fraction of CuFe<sub>2</sub>O<sub>4</sub> phase is only 28.33%, indicating that the annealing temperature of 700°C is not effective enough for the formation of tetragonal spinel phase. Only when the annealing temperature was up to 800 and 900°C, the diffraction peaks of CuFe<sub>2</sub>O<sub>4</sub> phase clearly intensified, corresponding to its mass fraction of 85.78 and 90.37%, respectively. The content of CuO tenorite phase also decreased whereas the characteristic peaks of hematite phase disappeared, suggesting the solid-state reaction between CuO and Fe<sub>2</sub>O<sub>3</sub> was promoted at high annealing temperatures. Moreover, at 800 and 900°C, the background noise of XRD patterns was reduced, the diffraction peaks became more symmetrical, which proves the enhanced crystallinity of CuFeO-800 and CuFeO-900 samples.

In order to investigate the influence of annealing temperatures on the morphology and the particle size of magnetic catalysts, FE-SEM characterization was used. As shown in Fig. 2a, the microstructure of CuFeO-700 sample mainly consists of irregularly polyhedral particles in the agglomerated state with the mean size ranging from 200 to 500 nm. When the annealing temperature rose to 800°C, a part of particles became large grains (500–1.5 μm) while some small submicroscopic particles are still observed (Fig. 2b). However, at the annealing temperature of 900°C, almost all these submicroparticles are replaced by the large grains with the average diameter of 1–4 μm (Fig. 2c), which can be related to the growth and the coalescence of particles at high temperatures. As a result, the BET surface area of our samples was found to dramatically decrease when the annealing temperature increased from 700 to 900°C (Table 2).

The FTIR spectra of our CuFeO samples are represented in Fig. 3. Both three spectra depict a broad absorption band at about 3400–3600 cm<sup>-1</sup>, ascribed to the stretching vibrations of surface hydroxyl groups or adsorbed water molecules [15]. They also show the metal-oxygen bands in the region of 385–600 cm<sup>-1</sup>. Generally, thanks to the geometrical configuration of spinel structure, the FTIR spectrum of CuFe<sub>2</sub>O<sub>4</sub> is characterized by two vibrational wavenumbers in this fingerprint region: the first peak situated at 385–

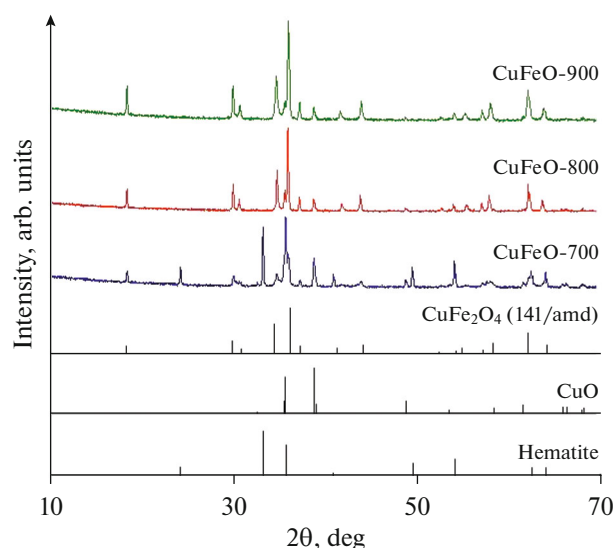


Fig. 1. XRD patterns of CuFeO-700, CuFeO-800, and CuFeO-900 samples.

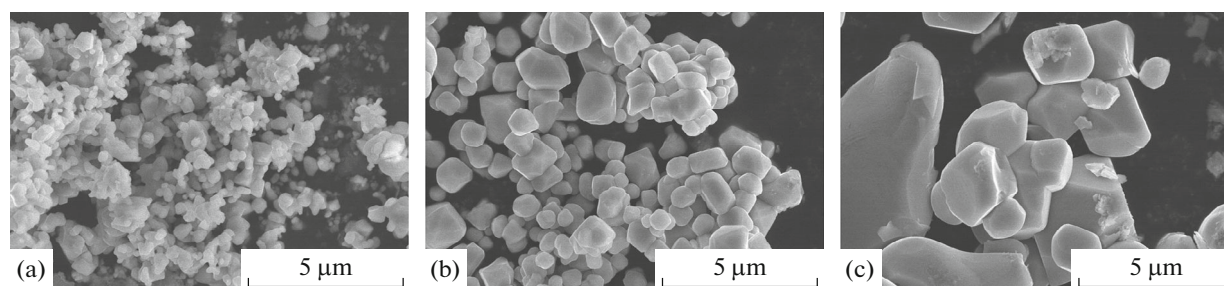


Fig. 2. FE-SEM micrographs of CuFeO-700 (a), CuFeO-800 (b), and CuFeO-900 (c) samples.

$450\text{ cm}^{-1}$  corresponds to the stretching vibrations of the metal–oxygen bonds in octahedral sites ( $M_{\text{octa}}\text{--O}$ ) and the second peak located in the range of  $550\text{--}600\text{ cm}^{-1}$  is attributed to the stretching vibrations of chemical bonds between tetrahedral metallic ions and oxygen ions ( $M_{\text{tetra}}\text{--O}$ ) [16]. These peaks are clearly observed in the FTIR spectra of CuFeO-800 (at  $431$  and  $594\text{ cm}^{-1}$ ) and CuFeO-900 samples (at  $435$  and  $600\text{ cm}^{-1}$ ), which is in good agreement with the superior content of  $\text{CuFe}_2\text{O}_4$  in their phase composition. Furthermore, the intensity of  $M_{\text{tetra}}\text{--O}$  peak is always much higher than that of  $M_{\text{octa}}\text{--O}$  peak, indicating the predominant presence of tetrahedral metallic ions on the surface of these catalysts. However, for CuFeO-700 sample, due to the low content of  $\text{CuFe}_2\text{O}_4$  phase (28.33%), only the  $M_{\text{tetra}}\text{--O}$  peak of spinel structure was detected at  $581\text{ cm}^{-1}$ . Instead of  $M_{\text{octa}}\text{--O}$  peak, a weak peak appeared at  $480\text{ cm}^{-1}$ , corresponding to the Fe–O bending vibration mode of  $\alpha\text{-Fe}_2\text{O}_3$  [17]. Besides, a new peak at  $1135\text{ cm}^{-1}$  can be attributed to the  $\text{CH}_2$  wagging vibrations from  $\text{CH}_3$  groups [18] or C–O stretching vibrations [19]. These new peaks indicate that the annealing at  $700^\circ\text{C}$  is not enough for the effective transfor-

Table 2. Specific surface area and magnetic parameters of CuFeO-700, CuFeO-800, and CuFeO-900 samples

Sample	$S_{\text{BET}}, \text{m}^2 \text{g}^{-1}$	$M_s, \text{emu g}^{-1}$	$H_c, \text{Oe}$	$M_r, \text{emu g}^{-1}$
CuFeO-700	1.468	9.56	363.19	3.60
CuFeO-800	1.453	25.75	362.89	8.57
CuFeO-900	0.740	29.89	4.26	3.53

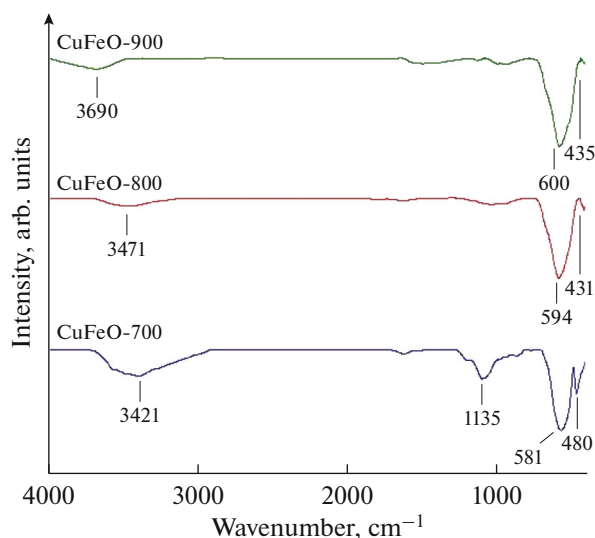


Fig. 3. FTIR spectra of CuFeO-700, CuFeO-800, and CuFeO-900 samples.

mation from metallic precursors to  $\text{CuFe}_2\text{O}_4$  and several organic species from tamarind fruit extract may still remain on the surface of CuFeO-700 sample.

#### Magnetic Properties

The hysteresis loop of our three samples is shown in Fig. 4a. Their magnetic parameters deduced from these loops are listed in Table 2. Both three CuFeO samples were found to follow the typical ferromagnetic behavior at room temperature. However, their magnetic parameters, especially the saturation magnetization ( $M_s$ ) and the coercivity ( $H_c$ ) were strongly affected by the annealing temperatures. In fact, among these materials, CuFeO-700 displayed the lowest  $M_s$  value ( $9.56 \text{ emu g}^{-1}$ ) which was only 37 and 32% of that of CuFeO800 ( $25.75 \text{ emu g}^{-1}$ ) and CuFeO-900 ( $29.89 \text{ emu g}^{-1}$ ), respectively. This evolution should be related to the annealing temperature dependence of crystal structure, phase composition and particle size. It is widely acknowledged that hematite phase and tenorite phase do not exhibit ferromagnetic properties [20, 21]. Hence, the low mass fraction of magnetic  $\text{CuFe}_2\text{O}_4$  phase (28.33%) in the phase composition of CuFeO-700 sample is one of the reasons for its little magnetism. Moreover, due to the minor particle size (200–300 nm), the total magnetic domain size of this sample is limited, which also restricts the number of atomic magnetic moments in the domain and then lessens the saturation magnetization. When the annealing temperature increased to 800 and 900°C, the content of  $\text{CuFe}_2\text{O}_4$  phase was markedly enhanced, the particle size was also increased, leading to the great increase in  $M_s$  value. As a consequence, CuFeO-800 and CuFeO-900 samples can be easily separated from the solution by a commercial magnet (Figs. 4c and 4d) whereas the magnetic separation seems to be ineffective for CuFeO-700 sample (Fig. 4b). Besides, owing to the enhancement of crystallinity and the decrease in impurity phase content ( $\text{Fe}_2\text{O}_3$  and CuO), the atomic magnetic moments of CuFeO-900 sample can easily rotate following the external magnetic field, inducing the significant reduction of  $H_c$  value. With the coercivity (4.06 Oe) inferior to 100 Oe, CuFeO-900 sample can be classified as a soft ferromagnetic material while the two other samples exhibit the hard ferromagnetic behavior. It should be noted that both three samples revealed the low  $M_r$  values, which allows them to be quickly re-dispersed in solution after the magnetic separation.

#### Heterogeneous Photo-Fenton Catalytic Activity

The heterogeneous photo-Fenton catalytic performance of our CuFeO samples was studied via the MB degradation in the presence of oxalic acid as a radical producing source. From the time-dependent curves of MB degradations (Figs. 5a and 5b), it was observed that our CuFeO samples can effectively accelerate the MB removal under both UVA light and visible light. Without these catalysts, the MB concentration relatively remained intact during 1 h of UVA light illumination and 3 h of visible light illumination, indicating that the direct self-photolysis of MB can be neglected in our systematic catalytic tests.

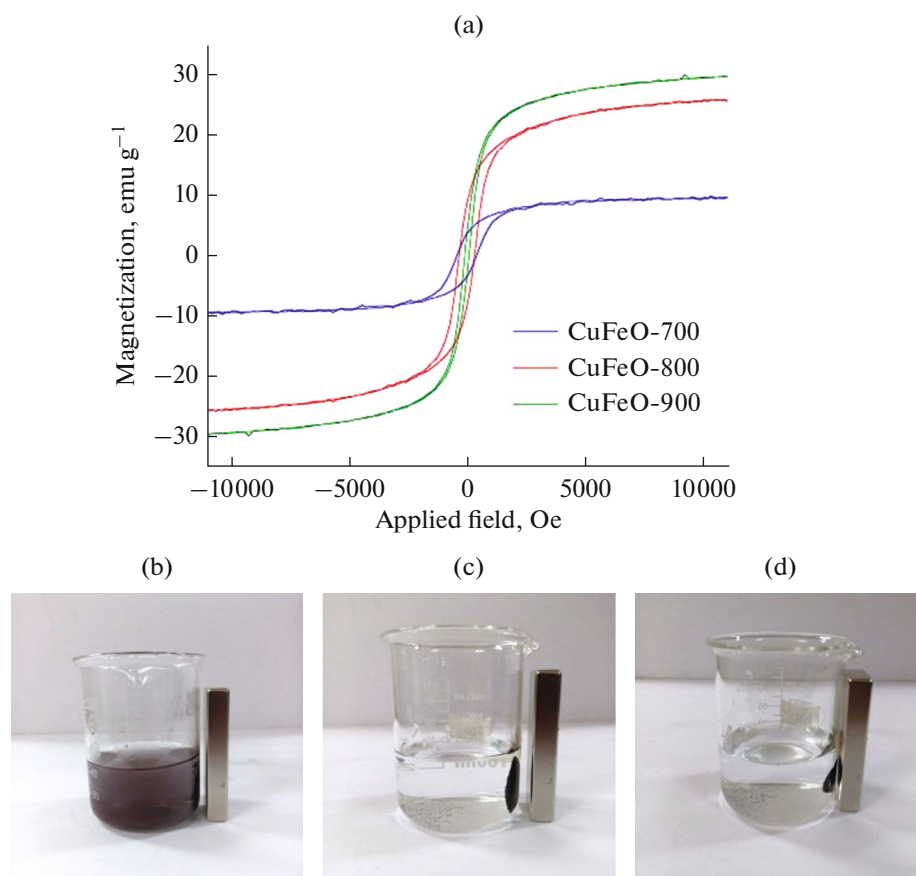


**Fig. 4.** Magnetic hysteresis at room temperature of CuFeO-700, CuFeO-800, and CuFeO-900 samples (a); photographs of magnetic separation for CuFeO-700 (b), CuFeO-800 (c), and CuFeO-900 (d) samples using a magnet.

Moreover, as shown in Figs. 5c and 5d, for both 3 magnetic catalysts, the natural logarithm plots of MB concentration ratios versus time are practically linear, which proves that the photo-Fenton MB degradation follows the pseudo-first-order Langmuir–Hinshelwood kinetic model. Hence, the photo-Fenton catalytic activity can be assessed towards the apparent rate constant ( $k$ ) of MB degradation (Table 3). Among our samples, the CuFeO-800 catalyst always showed the best performance with the highest rate constants ( $k = 2.01 \text{ h}^{-1}$  under UVA light and  $k = 0.28 \text{ h}^{-1}$  under visible light). For CuFeO-700 and CuFeO-900 samples, the rate constant was significantly reduced, which confirms the strong dependence of catalytic activity upon annealing temperatures. Moreover, the concentrations of  $\text{Fe}^{3+}$  and  $\text{Cu}^{2+}$  ions leached from CuFeO-800 (determined by AAS) sample during the photoFenton reactions were only 2.58 and 1.07 mg/L, respectively. These low concentrations suggest that the dissolution of metallic ions was negligible and that the MB degradation mainly comes from the heterogeneous catalytic activity of CuFeO-800 sample.

In addition, the reuse tests for CuFeO-800 catalyst were also performed to evaluate its reproducibility. Figure 6 shows the rate constant of MB degradation on this catalyst in four consecutive experiments under UVA light and under visible light. It was observed that the photo-Fenton catalytic performance of CuFeO-800 sample was only slightly reduced after three-time reuses, suggesting the high potential of this material for practical applications.

### Discussion

In our study, magnetic  $\text{CuFe}_2\text{O}_4$  powders were synthesized by the sol-gel method using tamarind fruit extract as a chelating agent. In order to elucidate the role of this fruit extract,  $\text{CuFe}_2\text{O}_4$  was also prepared from the solution containing  $\text{Fe}_2(\text{SO}_4)_3$  (0.5 mol/L) and  $\text{CuSO}_4$  (0.5 mol/L) by a simple coprecipitation method with NaOH as a precipitate agent, followed by an annealing at  $800^\circ\text{C}$  for 2 h (labelled as CuFeO-

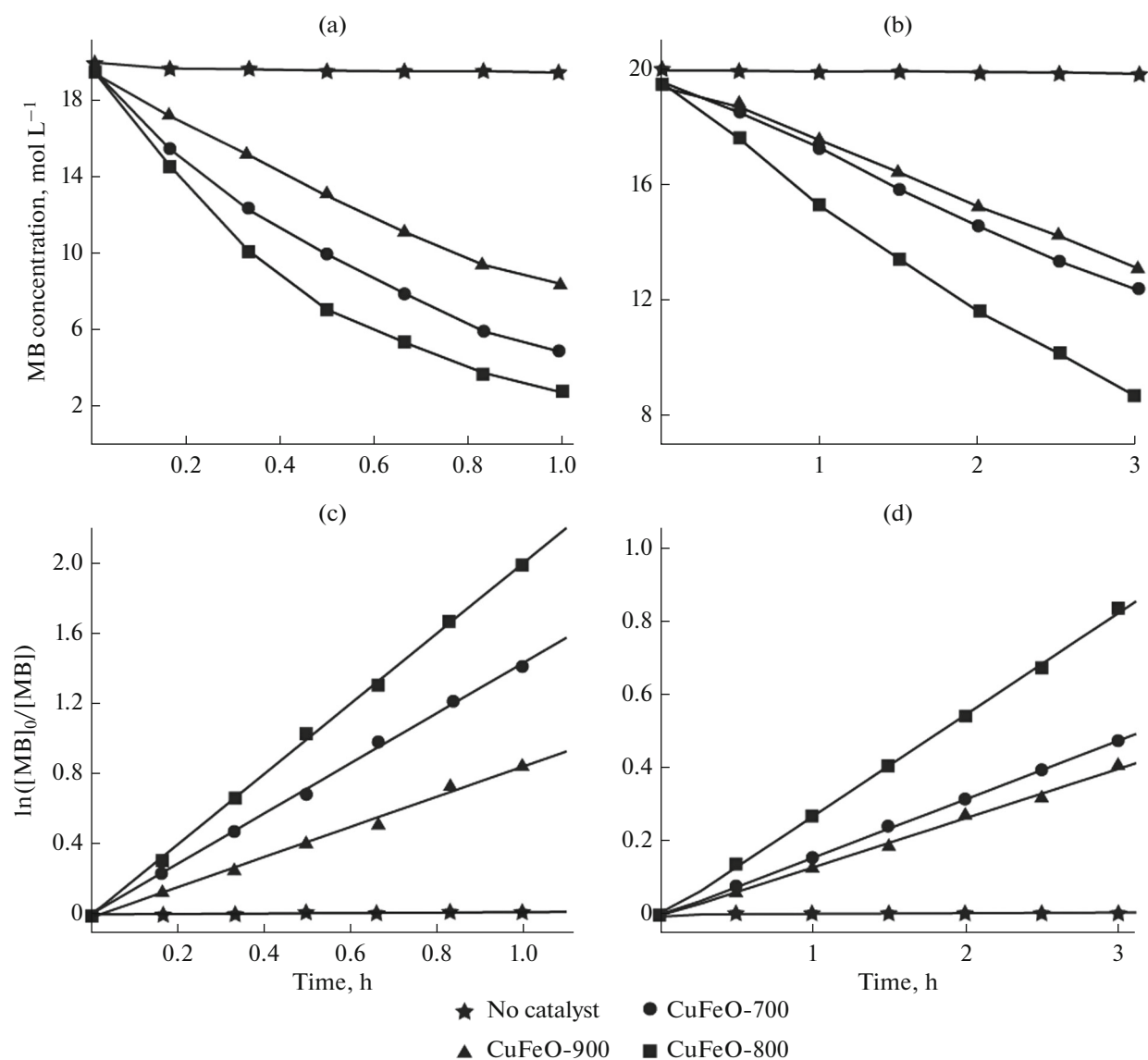


**Fig. 5.** Comparison of MB degradation on magnetic catalysts in the presence of oxalic acid: evolution of MB concentration as a function of time under UVA light (a) and visible light (b),  $\ln([MB]_0/[MB])$  versus time plot under UVA light (c) and visible light (d).  $[MB]$  is the MB concentration ( $\text{mol L}^{-1}$ ) at time  $t$  and  $[MB]_0$  is the initial MB concentration ( $\text{mol L}^{-1}$ ).

copre). Figure 7a represents its XRD patterns, in comparison with that of CuFeO-800 samples. Although the XRD pattern of CuFeO-copre also shows the characteristic peaks of CuFe<sub>2</sub>O<sub>4</sub> tetragonal spinel phase and CuO tenorite phase with the mass fractions (82.48 and 17.52%, respectively) close to those of CuFeO-800 sample, these diffraction peaks were clearly observed to be weak and asymmetrical, with a very unsta-

**Table 3.** Comparison of rate constants of MB degradation over catalysts under visible light and UVA light in the presence of oxalic acid

Rate constant of MB degradation $k$ ( $\text{h}^{-1}$ ) under light	Sample		
	CuFeO-700	CuFeO-800	CuFeO-900
Visible	0.16	0.28	0.13
UVA	1.43	2.01	0.86

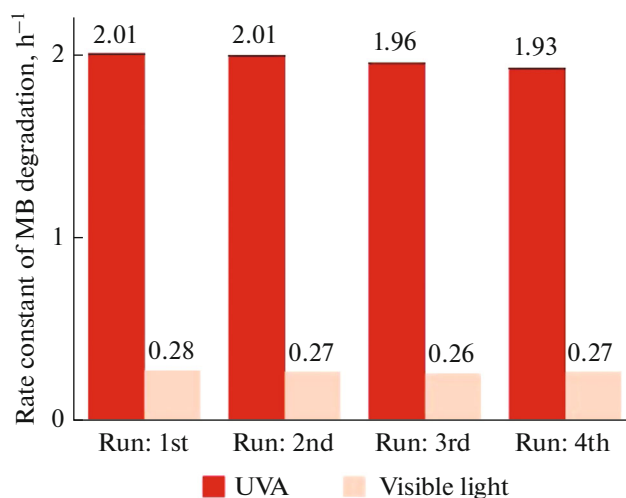


**Fig. 6.** Rate constants of MB degradation on CuFeO-800 sample in four consecutive experiments under UVA light and visible.

ble baseline, indicating the low crystallinity of CuFeO-copre sample. This result can be explained by the non-simultaneous formation of Fe(OH)<sub>3</sub> vs. Cu(OH)<sub>2</sub>, which makes Fe<sup>3+</sup> and Cu<sup>2+</sup> ions in each precipitate require a lot of energy to diffuse into each other. As a result, the annealing step at 800°C within 2 h is not enough to form CuFe<sub>2</sub>O<sub>4</sub> with high crystallinity. In contrast, since the ingredients in the tamarind fruit extract are able to form soluble polynuclear complexes with Fe<sup>3+</sup> and Cu<sup>2+</sup> ions, the sol-gel process using tamarind fruit extract was likely to produce a brown gel in which these ions were well dispersed into each other. Thereby, the annealing step at 800°C within 2 h did not only produce successfully CuFe<sub>2</sub>O<sub>4</sub> but also provided enough energy to improve its crystallinity, as proved by the XRD pattern of CuFeO-800. Interestingly, the photo-Fenton catalytic performance of CuFeO-800 was found to be impressively higher than that of CuFeO-copre under both UVA light and visible light (Fig. 7b). This demonstrates that the crystallinity of CuFe<sub>2</sub>O<sub>4</sub> plays an important role in the catalytic activity and can be controlled by using tamarind fruit extract.

Moreover, the annealing temperature used in sol-gel method was also an important factor affecting the catalytic performance of our ferrite samples. According to the literature [22], when using oxalic acid in the catalytic ferrite systems, the ferric ions on the surface of catalytic powders can react with oxalic acid to form ferrioxalate complexes. Under light excitation, these complexes can produce various reactive oxygen species, including hydroxyl radicals, which are able to mineralize almost all organic molecules. Therefore, the photo-Fenton performance induced by oxalic acid is expected to significantly depend on the surface Fe(III) content of catalysts. In our previous work [23], owing to the presence of ferric ions, both spinel structural CuFe<sub>2</sub>O<sub>4</sub> and hematite Fe<sub>2</sub>O<sub>3</sub> were found to exhibit good photo-Fenton catalytic performance. Even, Fe<sub>2</sub>O<sub>3</sub> showed better activity than CuFe<sub>2</sub>O<sub>4</sub> for the degradation of MB in the presence of oxalic acid. However, our CuFeO-700 sample in this study displayed considerably lower activity than CuFeO-800 sample although the hematite Fe<sub>2</sub>O<sub>3</sub> phase in the catalyst prepared at 700°C accounted for the highest mass fraction. This evolution of catalytic performance can be explained by the distribution of metal ions in octahedral and tetrahedral sites on the surface of spinel materials. From FTIR analysis results, the surface of three CuFeO catalysts is mainly occupied by the metallic ions at the tetrahedral sites, represented by the intense M<sub>tetra</sub>-O peak. When the annealing temperature of the tamarind fruit extract-assisted sol-gel method increased from 700 to 800°C, the M<sub>tetra</sub>-O peak tended to shift to higher wavenumbers, from 581 to 594 cm<sup>-1</sup>. It was widely acknowledged that the wavenumber of a bond vibration in FTIR spectra can be calculated by the following equation [24]:

$$W = \frac{1}{2\pi c} \sqrt{\frac{k}{\mu}} \quad (1)$$

where  $W$  is the wavenumber of this bond vibration (cm<sup>-1</sup>),  $c$  is the speed of light (cm s<sup>-1</sup>),  $k$  is the force constant (N cm<sup>-1</sup>), which is proportional to the bonding strength, and  $\mu$  is the reduced mass (kg) of diatomic A-B molecule, which follows Eq. (2):

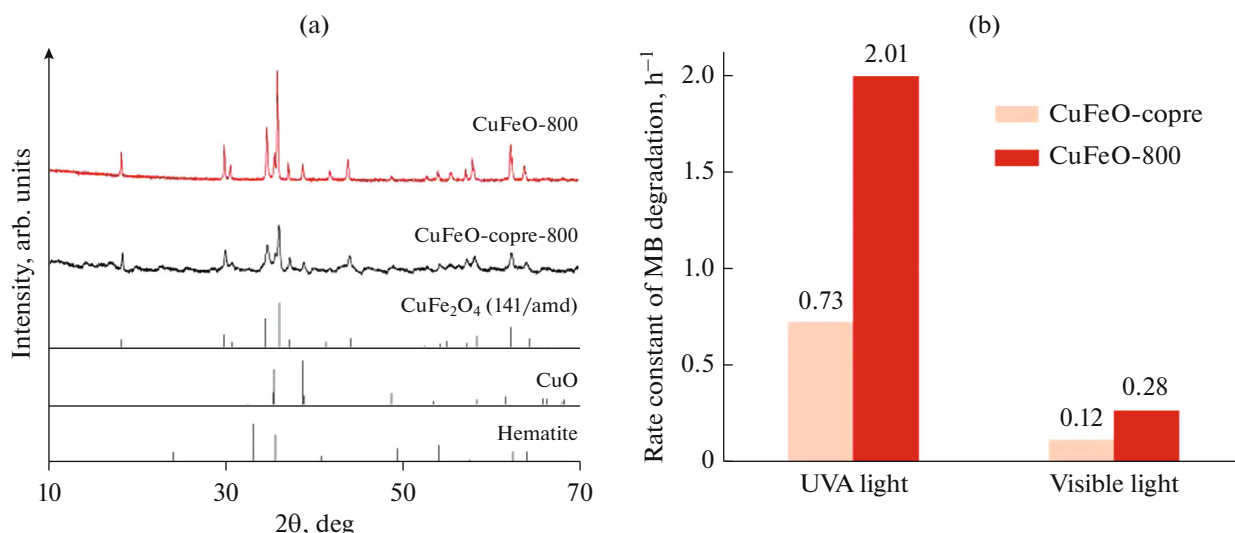


**Fig. 7.** Comparison of XRD patterns (a) and MB degradation rate constants (b) of CuFeO-copre and CuFeO-800 samples under UVA light and visible light.

$$\frac{1}{\mu} = \frac{1}{m_A} + \frac{1}{m_B} \quad (2)$$

Since the strength of  $\text{Fe}^{3+}-\text{O}^{2-}$  bond is superior to that of  $\text{Cu}^{2+}-\text{O}^{2-}$  bond [25] and the atomic weight of Fe is lower than that of Cu, the shift of  $M_{\text{tetra}}-\text{O}$  peak toward higher wavenumber in CuFeO-800 catalyst suggests the enhancement of  $\text{Fe}^{3+}$  content in surface tetrahedral sites, which improves the oxalic acid-induced catalytic performance. For CuFeO-700 catalyst, despite the fact that the mass fraction of hematite phase is high, the hematite component may exist in the inclusion body phase due to the uncomplete reaction of spinel formation at  $700^\circ\text{C}$ . As a result, the surface  $\text{Fe}^{3+}$  content of this sample is limited, which reduced the catalytic activity. In addition, the FTIR spectrum of CuFeO-700 still showed several organic species, derived from tamarind fruit extract, on its surface. These organic species may block the active sites and then decrease the MB removal.

For CuFeO-900 sample, the  $M_{\text{tetra}}-\text{O}$  peak continued to shift to higher wavenumber ( $600\text{ cm}^{-1}$ ), meaning that the surface  $\text{Fe}^{3+}$  content still increased. However, the photo-Fenton catalytic activities were found to decreased under both UVA light and visible light. The decline of catalytic performance should be attributed to the growth and the agglomeration of particles at high temperatures. In fact, the increase in annealing temperature from  $800$  to  $900^\circ\text{C}$  was likely to promote the growth of weld bonds between contacting microparticles, which enlarges the particles and consequently decreases the specific surface area (Table 2). As a result, the contact between oxalic acid and the active sites on the surface of catalysts was restricted, leading to the decline of photo-Fenton catalytic activities.

Despite the fact that our study only focused on evaluating the catalytic activity of ferrite powders through MB degradation, these catalysts were expected to be applied for the treatment of various organic dyes in textile wastewater owing to their ability to generate strongly oxidative and non-selective hydroxyl radicals, according to the photo-Fenton mechanism.

Moreover, since the discoloration of MB solution did not show any information about products of catalytic decomposition, the evolution of its total organic carbon (TOC) in the presence of CuFeO-800 catalyst was investigated. The TOC values were measured by Shimadzu TOCVCPH analyzer with a standard TOC solution prepared from potassium hydrogen phthalate for calibration. The results showed that the TOC value of MB solution effectively decreased from  $14.42$  to  $4.38\text{ mg/L}$  (after 1 h under UVA light) and to  $10.69\text{ mg/L}$  (after 3 h under visible light). Therefore, it can be concluded that the pollution level of MB solution was clearly reduced by using our CuFeO-800 catalyst.

## CONCLUSIONS

In our work, magnetic photo-Fenton catalysts based on  $\text{CuFe}_2\text{O}_4$  were successfully prepared by an environmentally friendly sol-gel method using tamarind fruit extract as a naturally available chelating agent. All synthesized samples showed photo-Fenton catalytic features for the degradation of Methylene Blue in the presence of oxalic acid under both UVA light and visible light. The effects of annealing temperatures on their magnetic properties and catalytic performance were also examined. When the annealing temperatures rose from 700 to 900°C, the mass fraction of tetragonal spinel  $\text{CuFe}_2\text{O}_4$  phase and the particle size strongly increased, which improves the magnetism of ferrite materials. Among three  $\text{CuFeO}$  samples, the  $\text{CuFeO}$ -800 catalyst, owing to the enhanced  $\text{Fe}^{3+}$  content on the surface, displayed the best photo-Fenton performance. At higher annealing temperatures, the growth of particles and the decrease in specific surface area are considered as the main reasons for the decline of catalytic activity.

## CONFLICT OF INTEREST

The authors declare that they have no conflicts of interest.

## REFERENCES

- Haija, M.A., Ayesh, A.I., Ahmed, S., and Katsiotis, M.S., Selective hydrogen gas sensor using  $\text{CuFe}_2\text{O}_4$  nanoparticle based thin film, *Appl. Surf. Sci.*, 2016, vol. 369, pp. 443–447.
- Jiang, J.Z., Goya, G.F., and Rechenberg, H.R., Magnetic properties of nanostructured  $\text{CuFe}_2\text{O}_4$ , *J. Phys.: Condens. Matter*, 1999, vol. 11, pp. 4063–4078.
- Zheng, M., Pengfei, G., and Fan, H., Mechanically enhanced magnetism in flexible semitransparent  $\text{CuFe}_2\text{O}_4$ /mica epitaxial heterostructures, *Appl. Surf. Sci.*, 2022, vol. 584, p. 152586.
- Sharma, R., Bansal, S., and Singhal, S., Tailoring the photo-Fenton activity of spinel ferrites ( $\text{MFe}_2\text{O}_4$ ) by incorporating different cations ( $\text{M} = \text{Cu, Zn, Ni}$  and  $\text{Co}$ ) in the structure, *RSC Adv.*, 2015, vol. 5, pp. 6006–6018.
- Guo, X., Xu, Y., Wang, K., Zha, F., Tang, X., and Tian, H., Synthesis of magnetic  $\text{CuFe}_2\text{O}_4$  self-assembled hollow nanospheres and its application for degrading Methylene Blue, *Res. Chem. Intermed.*, 2020, vol. 46, pp. 853–869.
- Dang, H.T., Nguyen, T.M.T., Nguyen, T.T., Thi, S.Q., Tran, H.T., Tran, H.Q., and Le, T.K., Magnetic  $\text{CuFe}_2\text{O}_4$  prepared by polymeric precursor method as a reusable heterogeneous Fenton-like catalyst for the efficient removal of Methylene Blue, *Chem. Eng. Commun.*, 2016, vol. 203, pp. 1260–1268.
- Gao, J., Wu, S., Han, Y., Tan, F., Shi, Y., Liu, M., and Li, X., 3D mesoporous  $\text{CuFe}_2\text{O}_4$  as a catalyst for photo-Fenton removal of sulfonamide antibiotics at near neutral pH, *J. Colloid Interface Sci.*, 2018, vol. 524, pp. 409–416.
- Noroozi, R., Gholami, M., Farzadkia, M., and Jafari, A.J., Catalytic potential of  $\text{CuFe}_2\text{O}_4$ /GO for activation of peroxymonosulfate in metronidazole degradation: Study of mechanisms, *J. Environ. Health Sci.*, 2020, vol. 18, pp. 947–960.
- Rashad, M.M., Mohamed, R.M., Ibrahim, M.A., Ismail, L.F.M., and Abdel-Aal, E.A., Magnetic and catalytic properties of cubic copper ferrite nanopowders synthesized from secondary resources, *Adv. Powder Technol.*, 2012, vol. 23, pp. 315–323.
- Dang, H.T., and Le, T.K., Precursor chain length dependence of polymeric precursor method for the preparation of magnetic Fenton-like  $\text{CuFe}_2\text{O}_4$ -based catalysts, *J. Sol-Gel Sci. Technol.*, 2016, vol. 80, pp. 160–167.
- Al-Hunaiti, A., Al-Said, N., Halawani, L., Haija, M.A., Baqaien, R., and Taher, D., Synthesis of magnetic  $\text{CuFe}_2\text{O}_4$  nanoparticles as green catalyst for toluene oxidation under solvent-free conditions, *Arab. J. Chem.*, 2020, vol. 13, pp. 4945–4953.
- Cahyana, A.H., Liandi, A.R., Yulizar, Y., Romdoni, Y., and Wendari, T.P., Green synthesis of  $\text{CuFe}_2\text{O}_4$  nanoparticles mediated by *Morus alba* L. leaf extract: Crystal structure, grain morphology, particle size, magnetic and catalytic properties in Mannich reaction, *Ceram. Int.*, 2021, vol. 47, pp. 21373–21380.
- Muzaffar, K., and Kumar, P., Tamarind—A mini review, *MOJ Food Process Technol.*, 2017, vol. 5, no. 3, pp. 296–297.
- Mindru, I., Gingasu, D., Patron, L., Ianculescu, A., Surdu, V.-A., Culita, D.C., Preda, S., Negut, C.-D., and Oprea, O., A new approach: Synthesis of cobalt aluminate nanoparticles using tamarind fruit extract, *Mater. Sci. Eng. B*, 2019, vol. 246, pp. 42–48.
- Kuroda, Y., Mori, T., Yagi, K., Makihata, N., Kawahara, Y., Nagao, M., and Kittaka, S., Preparation of visible-light responsive  $\text{TiO}_{2-x}\text{N}_x$  photocatalyst by a sol-gel method: Analysis of the active center on  $\text{TiO}_2$  that reacts with  $\text{NH}_3$ , *Langmuir*, 2005, vol. 21, no. 17, pp. 8026–8034.
- Guo, X., and Wang, D., Photo-Fenton degradation of Methylene Blue by synergistic action of oxalic acid and hydrogen peroxide with  $\text{NiFe}_2\text{O}_4$  hollow nanospheres catalyst, *J. Environ. Chem. Eng.*, 2019, vol. 7, p. 102814.

17. Wang, Y., Muramatsu, A., and Sugimoto, T., FTIR analysis of well-defined  $\alpha$ -Fe<sub>2</sub>O<sub>3</sub> particles, *Colloids Surf., A*, 1998, vol. 134, pp. 281–297.
18. Inkaya, E., Dincer, M., Korkusuz, E., and Yildirim, I., Molecular structure of 4-benzoyl-13-ethylcarboxylate 1-(4-methoxyphenyl)-5-phenyl-1*H*-pyrazole: A combined experimental and theoretical study, *J. Mol. Struct.*, 2012, vol. 1013, pp. 67–74.
19. Rafie, Sh.E., Shalaby, M.S., Zaher, F.M., Ramadan, R., and Abdel-halim, T.A., Precipitation of modified nano molecular magnesium oxide from bittern and ammonia, *Egypt. J. Chem.*, 2019, vol. 62, pp. 229–242.
20. Bhowmik, R.N. and Saravanan, A., Surface magnetism, Morin transition, and magnetic dynamics in antiferromagnetic  $\alpha$ -Fe<sub>2</sub>O<sub>3</sub> (hematite) nanograins, *J. Appl. Phys.*, 2010, vol. 107, p. 053916.
21. Karpenko, B.V., Kuznetsov, A.V., and Dyakin, V.V., On the magnetic susceptibility of tenorite, *J. Magn. Magn. Mater.*, 1996, vol. 152, pp. 116–122.
22. Liu, S.Q., Feng, L.R., Xu, N., Chen, Z.-G., and Wang, X.-M., Magnetic nickel ferrite as a heterogeneous photo-Fenton catalyst for the degradation of Rhodamine B in the presence of oxalic acid, *Chem. Eng. J.*, 2012, vol. 203, pp. 432–439.
23. Thi, T.U.T., Phan, V.H., Nguyen, H.T.P., Nguyen, T.L., Vu, A.N., and Le, T.K., Synthesis of magnetic CuFe<sub>2</sub>O<sub>4</sub>/Fe<sub>2</sub>O<sub>3</sub> core-shell materials and their application in photo-Fenton-like process with oxalic acid as a radical-producing source, *J. Asian Ceram. Soc.*, 2021, vol. 9, pp. 1091–1102.
24. Šolek, P., *Techincká Mechanika II* (Technical Mechanics II), Bratislava: Slov. Tech. Univ., 2009.
25. Brown, I.D., and Shannon, R.D., Empirical bond-strength–bond-length curves for oxides, *Acta Crystallogr., Sect. A*, 1973, vol. 29, pp. 266–282.